Supporting Information

Synthesis, characterization, and heparin-binding study of self-assembled *p*-cymene-Ru(II) metallocycle based on 4-amino-1,8-naphthalimide Tröger's base supramolecular scaffold

Binduja Mohan, and Sankarasekaran Shanmugaraju*

Department of Chemistry, Indian Institute of Technology Palakkad, Palakkad-678557, Kerala, India. E-mail: shanmugam@iitpkd.ac.in

---

Experimental section

Materials and methods

All reagents, solvents, and starting materials were purchased from Sigma-Aldrich and were used as received. Solvents used were HPLC grade unless otherwise stated. 4-Nitro-1,8-naphthalic anhydride, 4-Picolylamine, Palladium on carbon (10 wt% loadings), Hydrazine monohydrate (H_2N-$NH_2.H_2O$), Paraformaldehyde, Trifluoroacetic acid, Dichloro(*p*-cymene)ruthenium(II) dimer, 1,4-Dihydroxyanthraquinone and Silver trifluoromethanesulfonate were purchased from Sigma-Aldrich were reagent grade and used as received. Deuterated solvent $(CD_3)_2SO$, and CD_3CN used for NMR analyses were purchased from Sigma-Aldrich. *N*-[(4-pyridyl)methyl]-4-nitro-1,8-naphthalimide precursor and [(*p*-cymene)Ru(II)-(1,4-dihydroxy-9,10-anthracene-dione)Cl_2] were synthesized following the procedure reported in the literature.[1,2]

Electrochemical IA9000 digital melting point apparatus was used for measuring the melting point of ligands and metallocycles in an unsealed capillary tube. The Shimadzu Scientific Instruments (IR Tracer 100) equipped with an ATR sampler were used for recording the FT-IR spectra of ligands and metallocycles. All NMR spectra were recorded on a Bruker-DPX-Avance spectrometer operating at 400/600 MHz for ^{1}H NMR and 101/151 MHz for ^{13}C NMR in a

commercially available deuterated solvent. Chemical shifts are reported in parts-per-million (ppm) relative to the internal solvent [$(CD_3)_2SO$ or CD_3CN]. All NMR data were processed with Bruker Win-NMR 5.0, Topspin, and MestReNova software. Multiplicities were abbreviated as follows: singlet (s), doublet (d), doublet of doublet (dd), triplet (t), and multiplet (m). APCI-ESI mass spectra were acquired on a Bruker microTOF-Q III spectrometer interfaced to a Dionex UltiMate 3000 LC or direct insertion probe. The instrument was operated in positive or negative mode as required. The *m/z* values were recorded over a range of 100-2000. HPLC-grade CH_3CN or CH_3OH or DMSO were used as carrier solvents. All the UV-Visible spectra were recorded on a Thermo Scientific evolution 201 spectrometer using a 1 cm quartz cuvette. The emission spectra were measured on Perkin Elmer-6500 Fluorimeter and all the spectra were recorded at room temperature. All the UV and fluorescence spectral data were plotted using OriginPro 8.5.

Synthesis and Characterization

***N*-[(4-pyridyl)methyl]-4-amino-1,8-naphthalimide (Nap):** *N*-[(4-pyridyl)methyl]-4-nitro-1,8-naphthalimide (200 mg, 0.60 mmol) was stirred with 10% Pd/C in ethanol (15 mL) at room temperature for 5 minutes. To the solution, an excess of hydrazine monohydrate (2 mL) was added dropwise while stirring. The color of the reaction mixture changed immediately from black to dark green within a minute and the mixture was irradiated in the microwave at 100°C for 1 h. The resulting yellowish-green reaction mixture was filtered through celite and washed several times with fresh DMF until the washings ran clear. The combined filtrate was kept under reduced pressure to remove the solvents. The expected product **Nap** (146 mg, 80 %) was isolated as bright yellow solid after trituration with cold-diethyl ether. Melting point 250–252 ºC (decomp.). HRMS (APCI) *m/z*: calcd for $C_{18}H_{14}N_3O_2$ [$M+H^+$] 304.1086, found 304.1089; ^1H NMR (400 MHz, $(CD_3)_2SO$) δ 8.68-8.66 (1H, d, J = 8.0 Hz, Nap-H), 8.48-8.45 (3H, dd, J = 12.0 Hz, Nap-H, Pyridyl-

H), 8.24-8.22 (1H, d, *J* = 8.4 Hz, Nap-H), 7.71-7.69 (1H, t, *J* = 7.6 Hz, Nap-H), 7.56 (2H, s, Nap-NH_2), 7.28-7.27 (2H, d, *J* = 5.2 Hz, Pyridyl-H), 6.89-6.87 (1H, d, *J* = 8.4 Hz, Nap-H), 5.24 (2H, s, Pyridyl-CH_2); ^{13}C NMR (101 MHz, $(CD_3)_2SO$) δ 164.30, 163.27, 153.57, 150.02, 147.29, 134.78, 131.83, 130.38, 130.14, 124.51, 122.48, 121.92, 119.85, 108.74, 107.49, 58.13; FTIR υ_{max} (ATR, cm^{-1}) 3372, 3178, 2917, 2850, 1664, 1632, 1611, 1603, 1579, 1528, 1476, 1405, 1380, 1356, 1331, 1304, 1246, 1233, 1171, 1141, 1092, 1064, 1001, 991, 946, 878, 851, 835, 810, 796, 776, 756, 724, 677, 660, 647, 625, 607, 573, 561, 549, 540, 533, 524.

Bis-[*N*-(4-pyridyl)methyl)]-9,18-methano-1,8-naphthalimide-[*b,f*][1,5]diazocine (TBNap): Compound **Nap** (150 mg, 0.49 mmol, 1 equiv.) and paraformaldehyde (22 mg, 0.74 mmol, 1.5 equiv.) were flushed with argon. Trifluoroacetic acid (4 mL) was added at 0°C and the solution was stirred at room temperature for 12 h under an argon atmosphere. The reaction mixture was added dropwise to aqueous ammonium hydroxide (50 mL) at 0°C and ammonia solution was added until a pH > 11 was achieved. The residue was extracted in dichloromethane (200 mL) and the organic layer was washed successively with saturated $NaHCO_3$ (2 × 50 mL), brine (2 × 50 mL), and H_2O (2 × 50 mL). The solution was dried over $MgSO_4$ and the solvents were removed under reduced pressure to isolate the compound **TBNap** (172 mg, 0.27 mmol, 55 %) as an orange powder after trituration with cold-diethyl ether. Melting point 235–237 ºC (decomp.). HRMS (APCI) *m/z*: calcd for $C_{39}H_{27}N_6O_4$ $[M+H^+]$ 643.2094, found 643.2074; ^{1}H NMR (400 MHz, $(CD_3)_2SO$) δ 8.75 (2H, d, *J* = 8.0 Hz, Nap-H), 8.61-8.59 (6H, dd, *J* = 7.6 Hz, Nap-H, pyridyl-H), 8.10 (2H, s, Nap-H), 7.91-7.87 (2H, t, *J* = 15.6 Hz, Nap-H), 7.61-7.59 (4H, d, *J* = 4.8 Hz, pyridyl-H), 5.38 (4H, s, Pyridyl-CH_2), 5.17 (2H, d, *J* = 16.8 Hz, NCH_2), 4.70 (2H, s, NCH_2), 4.60 (2H, d, *J* = 16.8 Hz, NCH_2); ^{13}C NMR (101 MHz, $(CD_3)_2SO$) δ 163.99, 163.46, 152.50, 150.07, 144.87, 131.78, 131.25, 129.71, 128.42, 127.45, 127.43, 125.57, 124.92, 122.33, 118.00, 66.93, 57.19, 42.58; FTIR

υ_{max} (ATR, cm^{-1}) 2982, 2965, 1698, 1655, 1598, 1573, 1510, 1455, 1402, 1376, 1352, 1334, 1310, 1256, 1230, 1168, 1144, 1132, 1088, 1066, 1052, 1025, 1012, 994, 963, 948, 916, 873, 835, 805, 783, 762, 699, 682, 664, 608, 585, 549, 531.

Synthesis of metallocycle (TBNap-Ru-MC): The chloro-derivative of acceptor, (*p*-cymene)Ru(II)-(1,4-dihydroxy-9,10-anthracene-dione)Cl_2 (20 mg, 0.1 mmol), was stirred with 2.2 equivalent of $AgCF_3SO_3$ (56.5 mg, 0.22 mmol) at room temperature for about 2h in methanol in dark. The resultant solution was filtered through celite to remove the precipitated AgCl. To the clear green-colored filtrate, the dipyridyl donor **TBNap** (16.4 mg, 0.1 mmol) was added and stirred for 24 h at room temperature. The solvent in the mixture was then dried under vacuum and the residue was extracted in dichloromethane (10 mL), and then filtered, dried, and triturated in the cold-diethyl ether which resulted in the formation of a shiny dark-green colored self-assembled metallocycle **TBNap-Ru-MC**. Isolated yield = 58%. Melting point = 228-230°C (decomp.). ESI-MS (*m/z*): 1501.2 $[M–2OTf^-]^{2+}$, 950.7 $[M–3OTf^-]^{3+}$, 676.12 = $[M−4OTf^-]^{4+}$. ^{1}H NMR (600 MHz, CD_3CN) δ 8.62-8.59 (4H, dd, J = 18 Hz, Nap-H), 8.53-8.51 (8H, dd, J = 12 Hz, Pyridyl-H), 8.43-8.42 (4H, d, J = 6 Hz, Nap-H), 8.41-8.40 (4H, d, J = 12 Hz, Nap-H), 8.39 (4H, s, Nap-H), 8.32-8.29 (8H, dd, J = 12 Hz, Nap-H), 8.26-8.24 (4H, dd, J = 6 Hz, Nap-H), 8.09-8.07 (4H, dd, J = 18 Hz, Nap-H), 8.02-8.00 (4H, dd, J = 6 Hz, Ant-H), 7.94-7.92 (4H, dd, J = 6 Hz, Ant-H), 7.86-7.84 (4H, t, J = 6 Hz, Nap-H), 5.78-5.76 (8H, d, J = 6 Hz, Cymene-H), 5.73-5.72 (8H, d, J = 6 Hz, Cymene-H), 5.57, 5.55 (8H, d, J = 6 Hz, Cymene-H), 5.54-5.52 (8H, d, J = 6 Hz, Cymene-H), 5.10-5.08 (4H, d, J = 6 Hz, dizaocine-H), 5.01 (4H, s, dizaocine-H), 4.88-4.86 (4H, d, J = 6 Hz, dizaocine-H), 2.90-2.86 (4H, m, Cymene-H), 2.84 (12H, s, Cymene-H), 1.34-1.31 (24H, d, Cymene-H). ^{13}C NMR (151 MHz, CD_3CN) δ 170.55, 169.49, 163.81, 163.29, 152.12, 151.72, 150.66, 149.56, 137.64, 137.53, 136.49, 134.66, 133.24, 133.13, 132.99, 130.64, 129.42, 129.08,

128.05, 127.33, 127.17, 127.06, 126.76, 126.47, 126.07, 124.36, 123.55, 123.48, 122.46, 122.23, 120.11, 109.71, 109.63, 103.37, 102.85, 99.02, 85.13, 84.03, 83.95, 83.87, 83.80, 83.52, 83.32, 83.17, 82.75, 82.09, 82.38, 82.26, 65.52, 36.83, 42.27, 41.35, 30.43, 21.55, 21.48, 21.38, 21.28, 21.23, 16.63, 16.53. FTIR υ_{max} (ATR, cm^{-1}) 3502, 3070, 2962, 1697, 1658, 1597, 1535, 1458, 1404, 1249, 1149, 1026, 979, 918, 848, 787, 756, 717, 686, 632, 571, 517, 455.

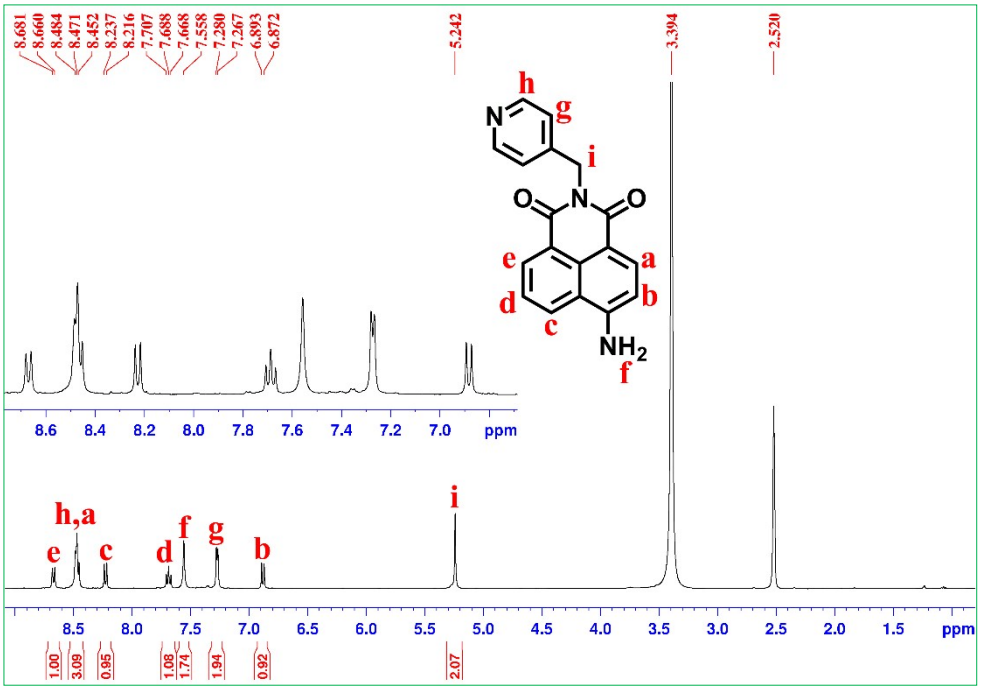

Fig. S1. ^{1}H NMR spectrum of **Nap** (400 MHz, DMSO-d_6).

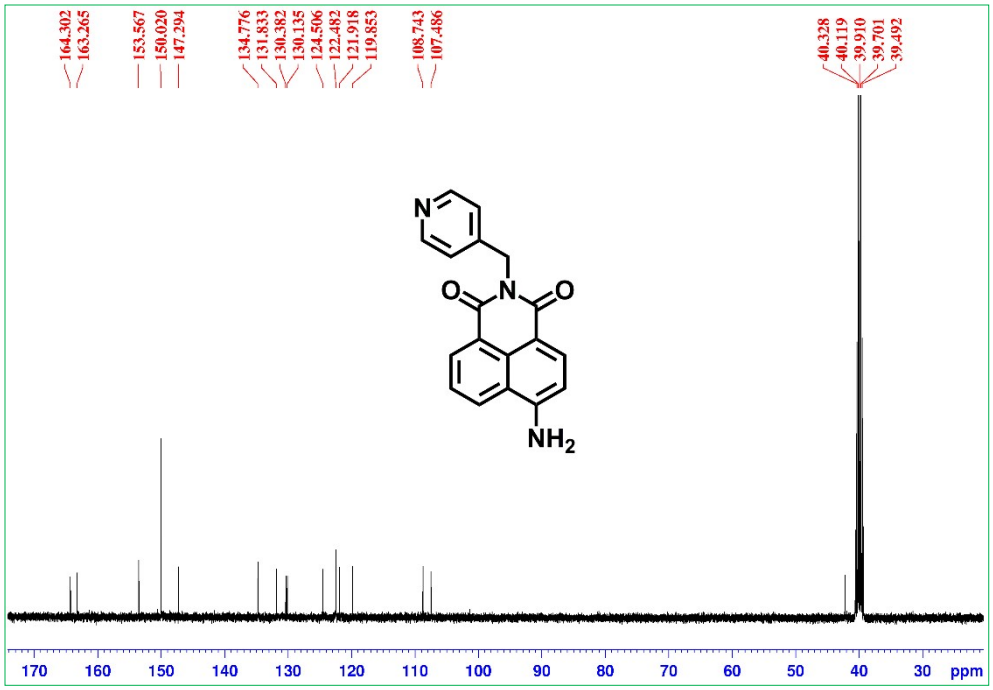

Fig. S2. ^{13}C NMR spectrum of **Nap** (101 MHz, DMSO-d_6).

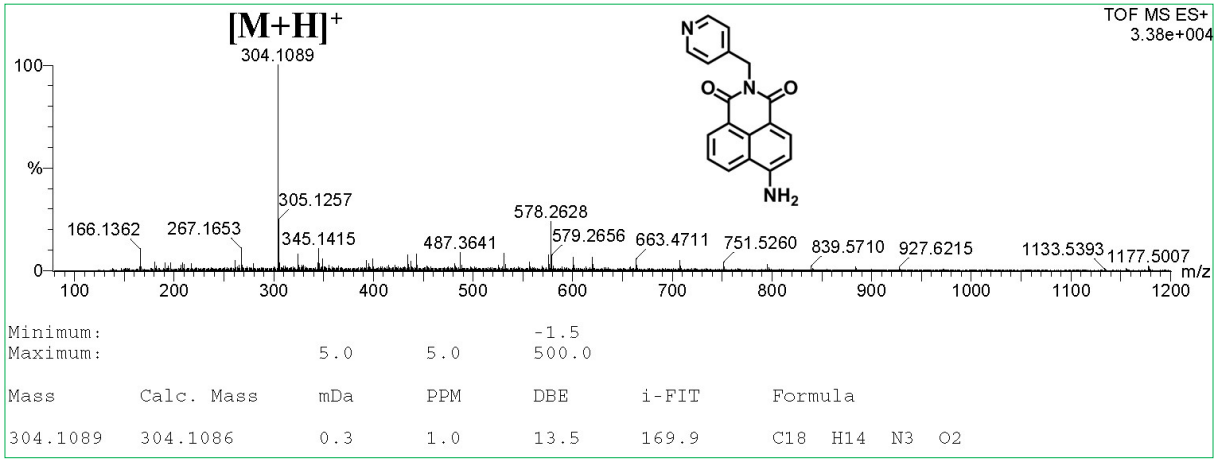

Fig. S3. HRMS spectrum of **Nap**.

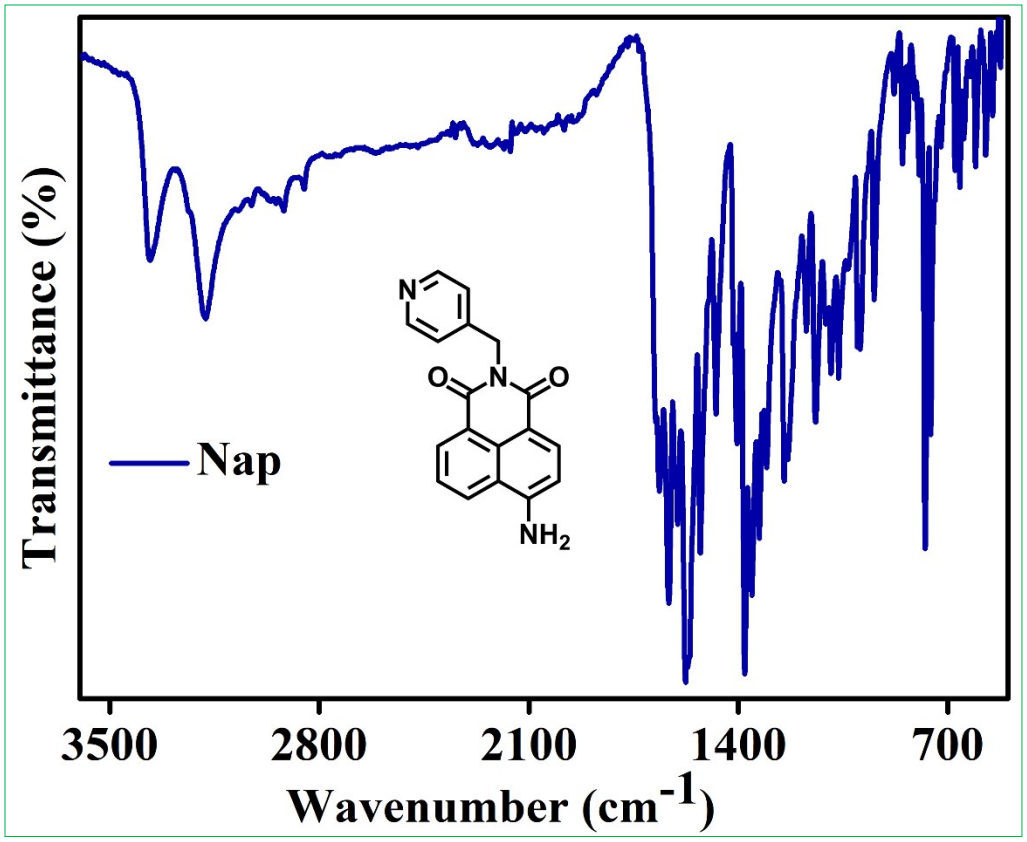

Fig. S4. FTIR spectrum of **Nap**.

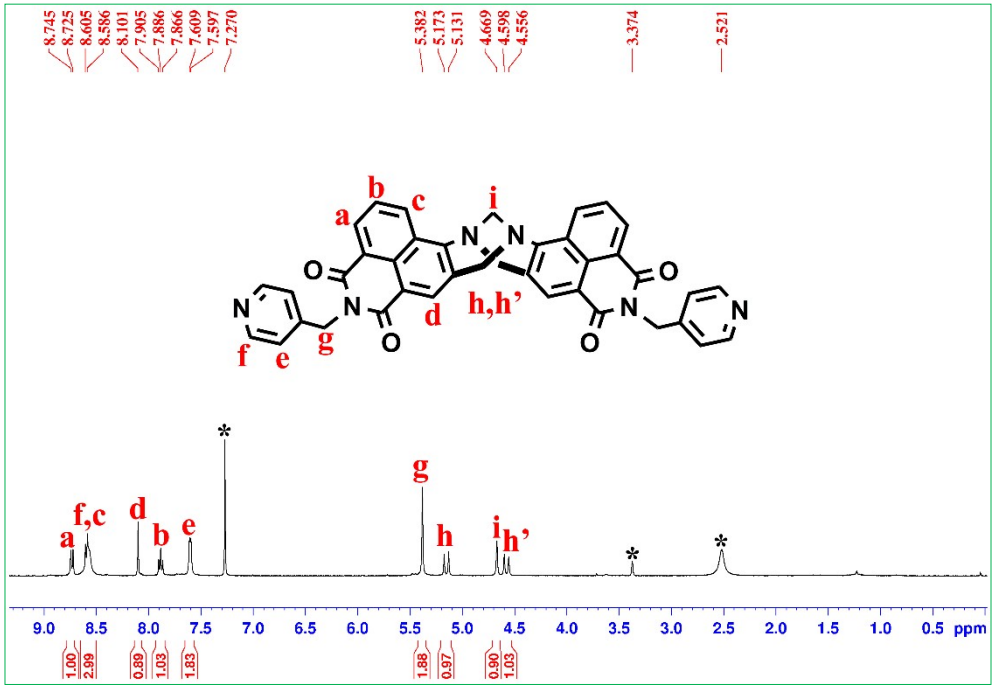

Fig. S5. ^{1}H NMR spectrum of **TBNap** (400 MHz, DMSO-d_6). *solvent residual peaks.

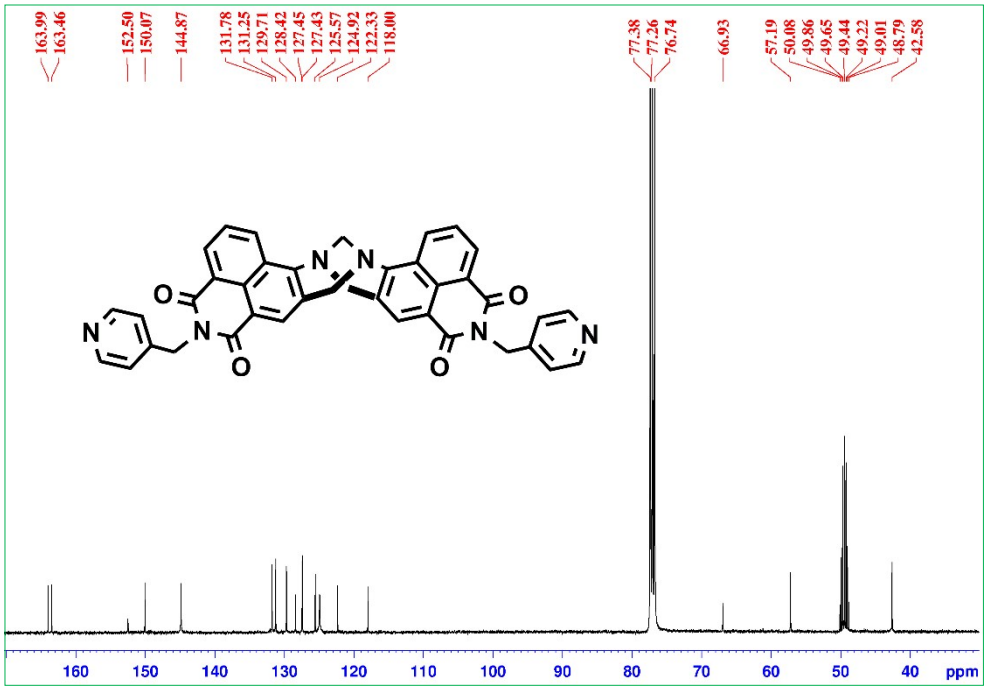

Fig. S6. ^{13}C NMR spectrum of **TBNap** (400 MHz, DMSO-d_6).

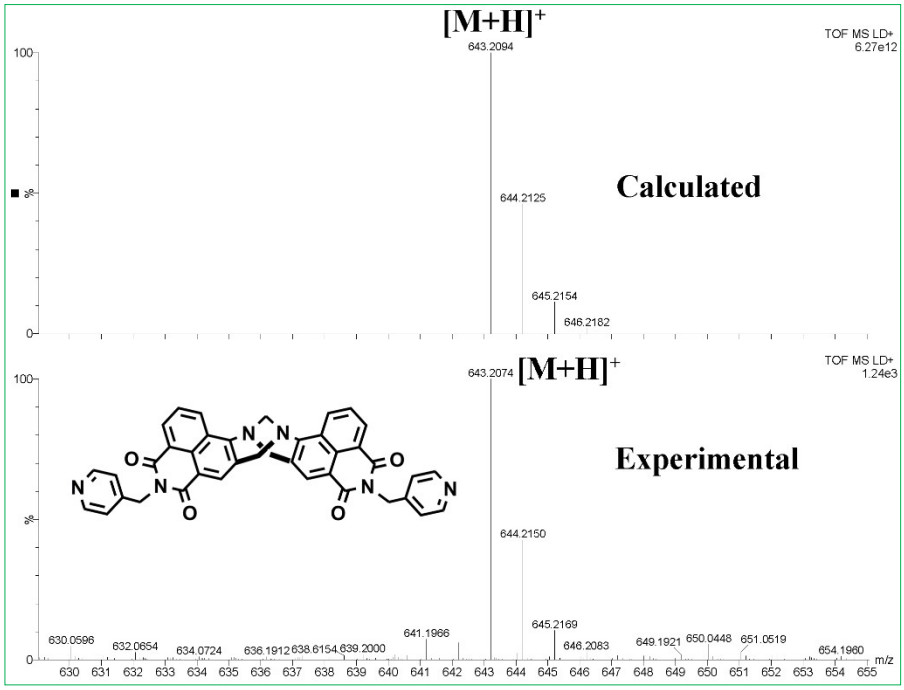

Fig. S7. Calculated and experimental HRMS spectrum of **TBNap**.

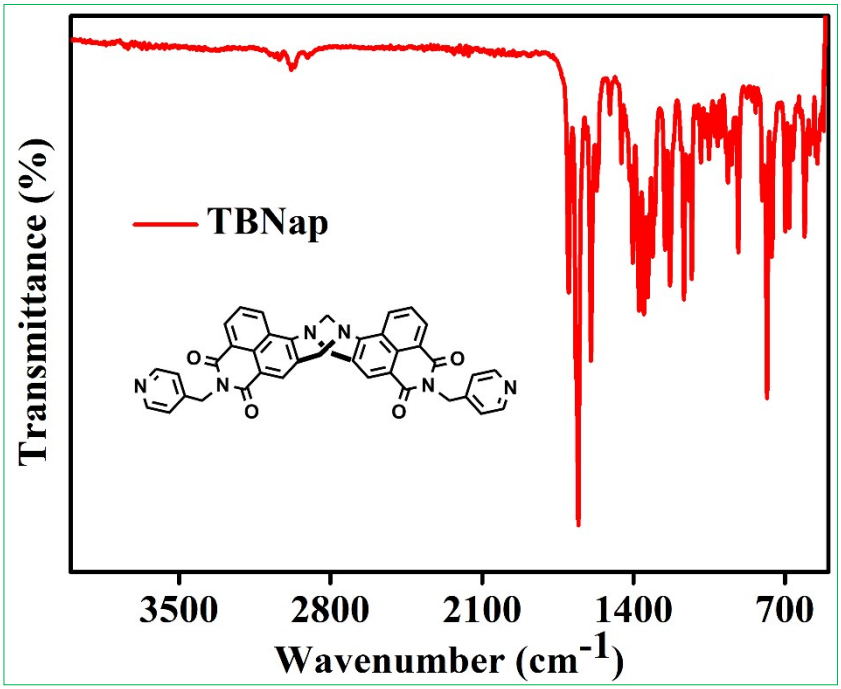

Fig. S8. FTIR spectrum of **TBNap**.

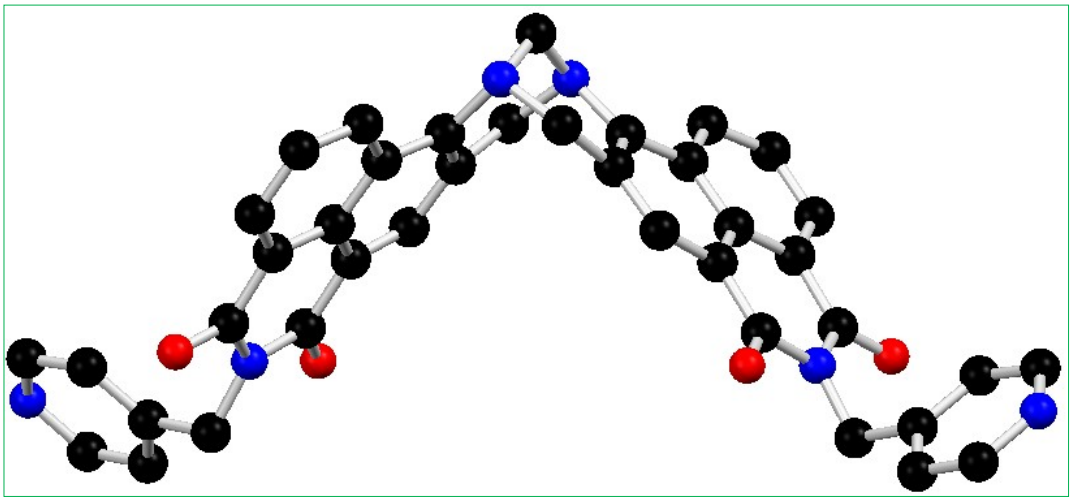

Fig. S9. Optimized structure of **TBNap** (Color code: Black C, Red O, and Blue N). Hydrogen atoms are omitted for clarity.

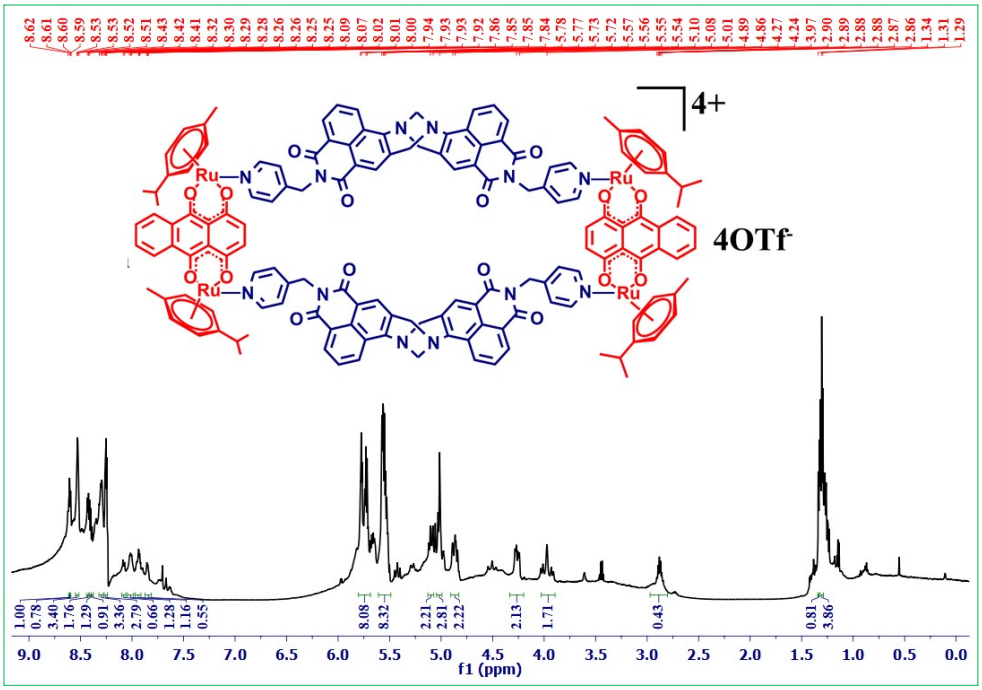

Fig. S10. ^{1}H NMR spectrum of **TBNap-Ru-MC** (600 MHz, CD_3CN). The solvent residual peaks were suppressed for clarity. The presence of several low-intense peaks is due to the racemic mixture of metallocycles since **TBNap** was a racemic mixture. Also, the significant spectral broadening is due to the formation of cage-like structures driven by metal-ligand coordination bonding interactions.

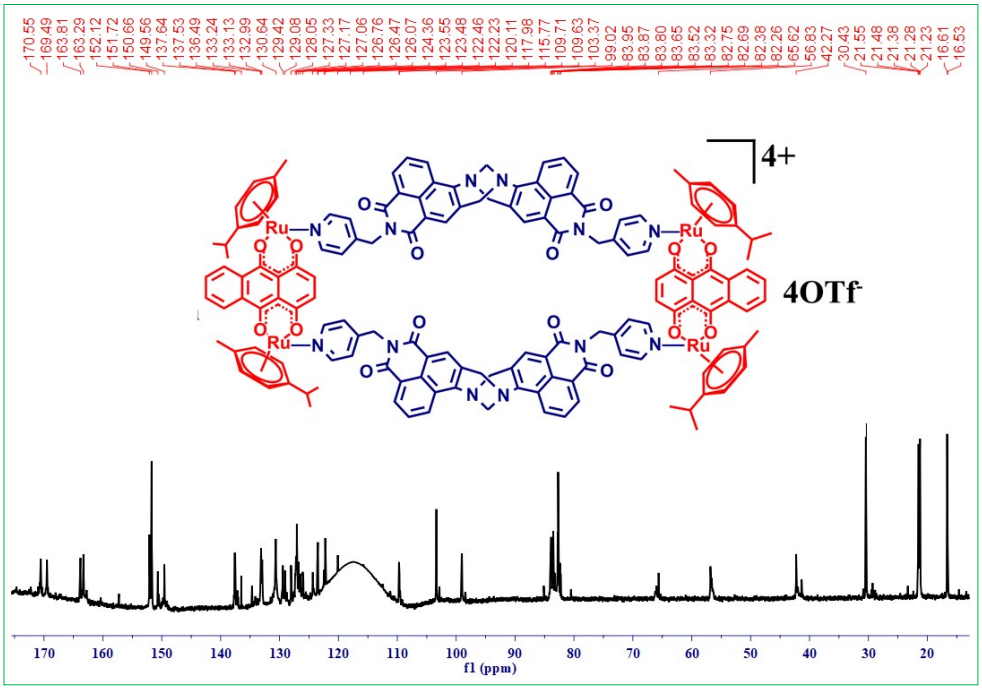

Fig. S11. ^{13}C NMR spectrum of **TBNap-Ru-MC** (151 MHz, CD_3CN). The solvent residual peaks are suppressed to visualize the compound peaks.

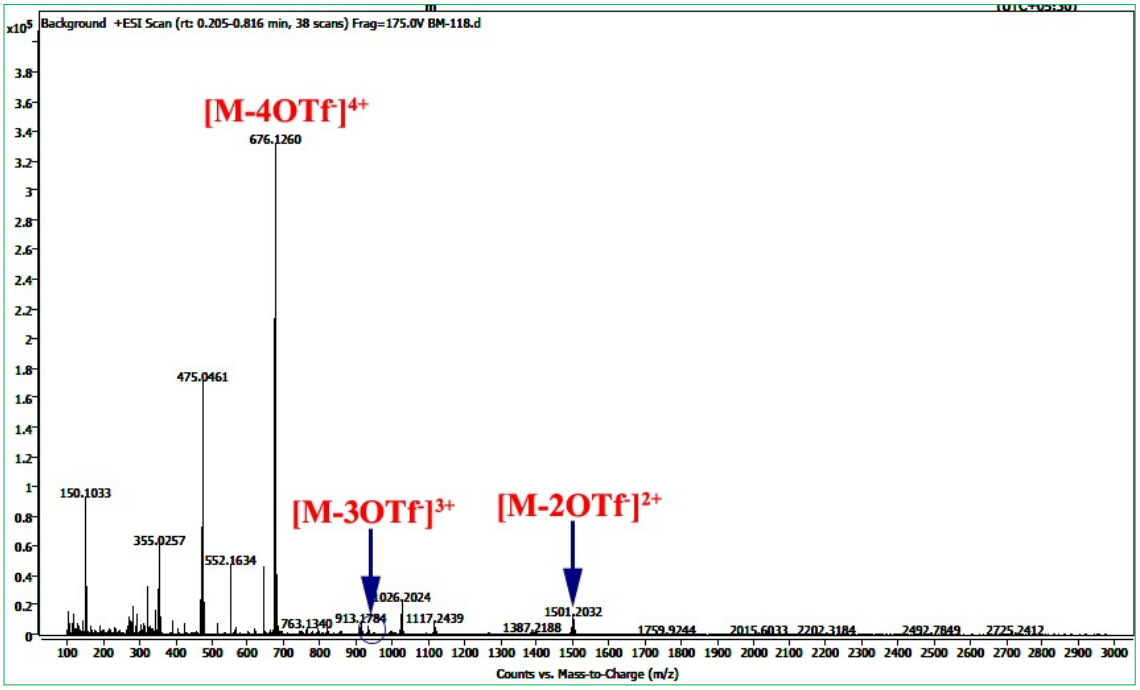

Fig. S12. ESI-MS spectrum of **TBNap-Ru-MC**.

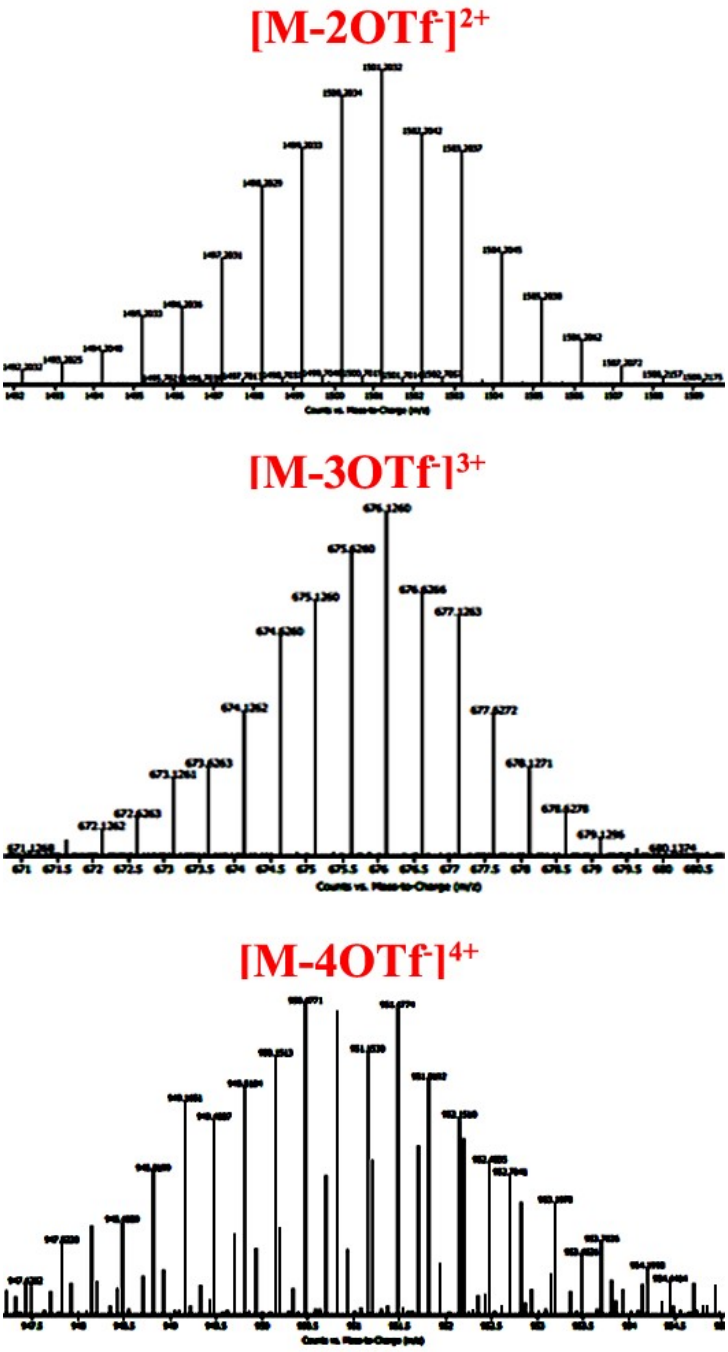

Fig. S13. The experimentally observed isotopic distributions corresponding to $\mathbf{M}^{2+}$, $\mathbf{M}^{3+,}$ and $\mathbf{M}^{4+}$ charged states of **TBNap-Ru-MC**.

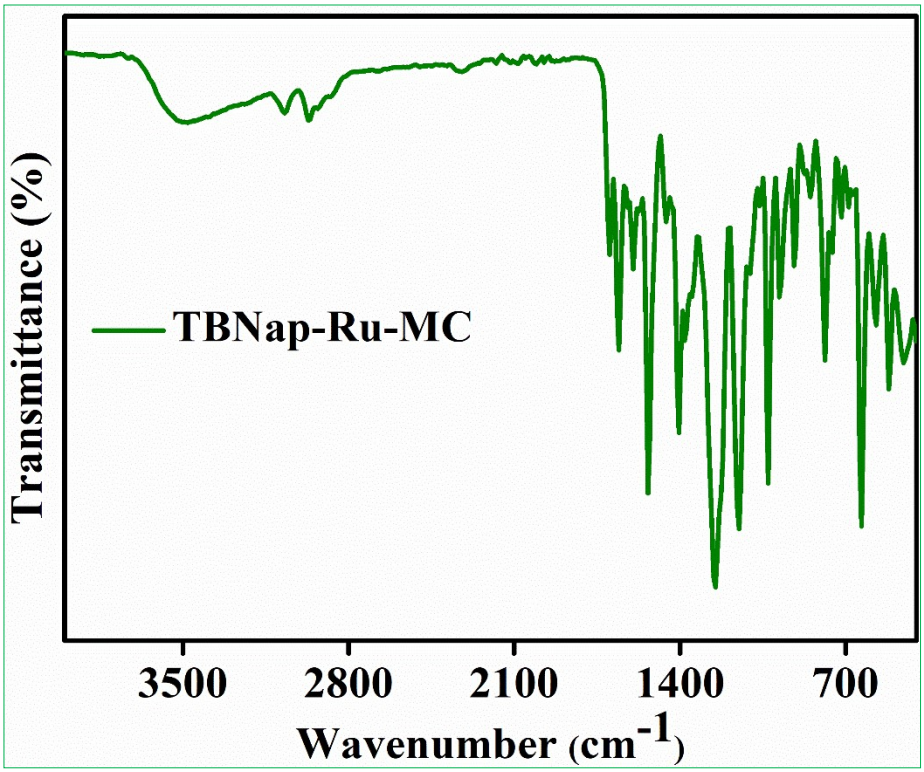

Fig. S14. FTIR spectrum of **TBNap-Ru-MC**.

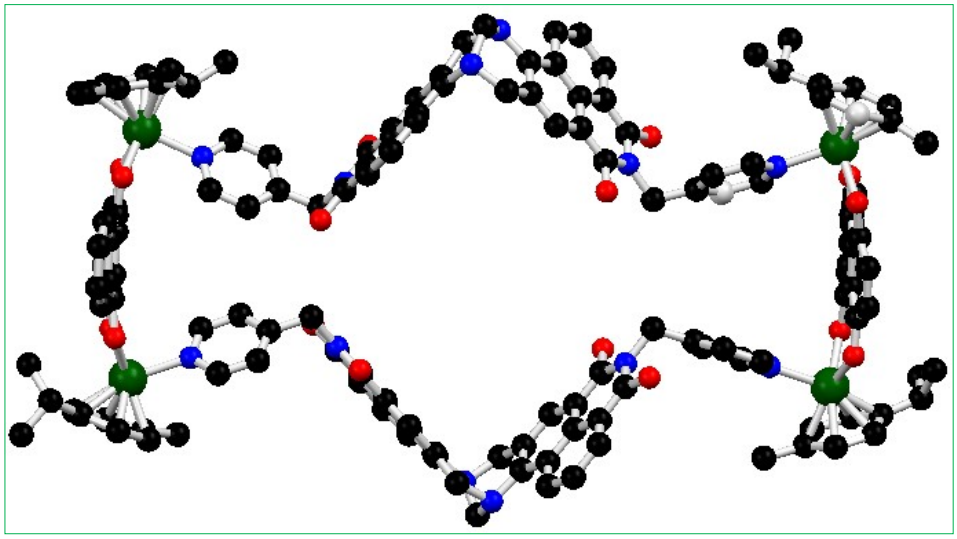

Fig. S15. Optimized structure of **TBNap-Ru-MC** (Colour code: Black C, Red O, and Blue N). Hydrogen atoms are omitted for clarity.

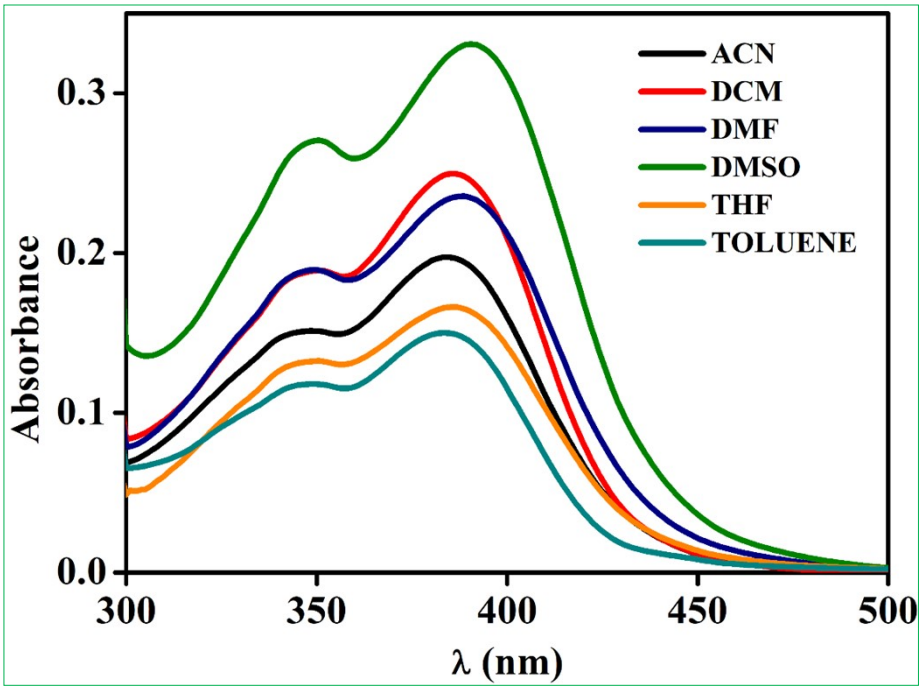

Fig. S16. UV-visible absorption spectra of **TBNap** in different solvents.

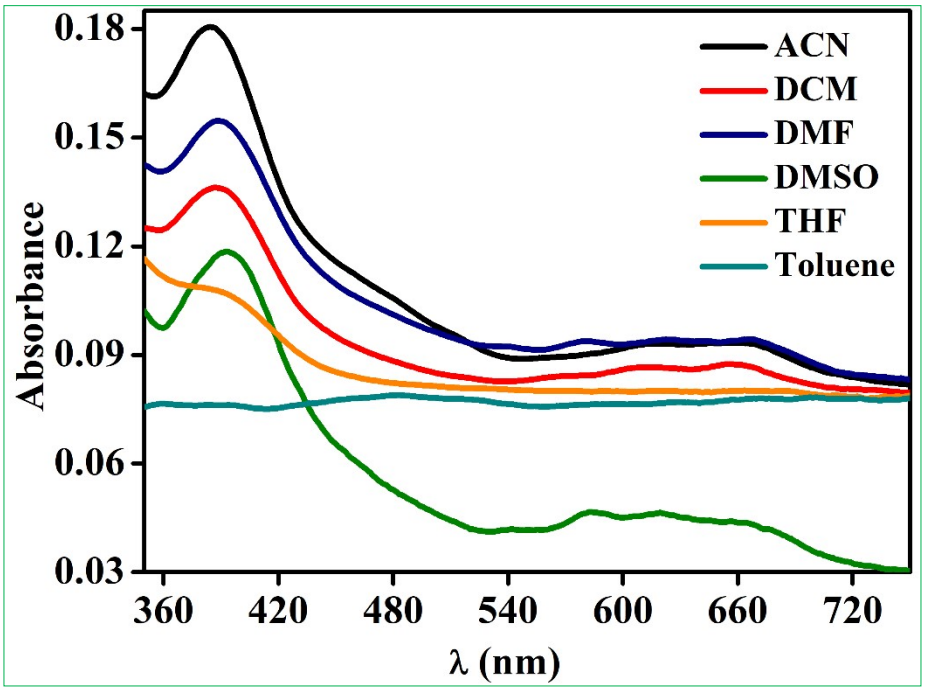

Fig. S17. UV-visible absorption spectra of **TBNap-Ru-MC** in different solvents.

References:

1. S. Shanmugaraju, C. S. Hawes, A. J. Savyasachi, S. Blasco, J. A. Kitchen and T. Gunnlaugsson, *Chem. Commun*., 2017, **53**, 12512-12515.

2. N. P. E. Barry, J. Furrer and B. Therrien, *Helv. Chim. Acta*., 2010, **93**, 1313-1328.